Vol 17 No 7, July 2008
1674-1056/2008/17(07)/2499-05

Chinese Physics B

© 2008 Chin. Phys. Soc.
and IOP Publishing Ltd

The theoretic analysis of maskless surface plasmon resonant interference lithography by prism coupling*

Fang Liang(方 亮)[a], Du Jing-Lei(杜惊雷)[a]†, Guo Xiao-Wei(郭小伟)[a], Wang Jing-Quan(王景全)[a], Zhang Zhi-You(张志友)[a], Luo Xian-Gang(罗先刚)[b], and Du Chun-Lei(杜春雷)[b]

[a] *Physics Department, Sichuan University, Chengdu* 610064, *China*
[b] *Institute of Optics and Electronics, Chinese Academy of Sciences, Chengdu,* 610209, *China*

(Received 5 October 2007; revised manuscript received 16 November 2007)

The use of an attenuated total reflection-coupling mode of prism coated with metal film to excite the interference of the surface plasmon polaritons (SPPs) was proposed for periodic patterning with a resolution of subwavelength scale. High intensity of electric field can be obtained because of the coupling between SPPs and evanescence under a resonance condition, which can reduce exposure time and improve contrast. In this paper, several critical parameters for maskless surface plasmon resonant lithography are described, and the preliminary simulation based on a finite difference time-domain technique agrees well with the theoretical analysis, which demonstrates this scheme and provides the theoretical basis for further experiments.

Keywords: surface plasmon polaritons (SPPs), enhancement, interference lithography, resolution
PACC: 4200, 4230H

1. Introduction

Since the integrated electrocircuit was first invented, the number of transistors that can be placed on a single chip has been increased rapidly according to Moore's law.[1] The characteristic dimension of pattern shrank from several micron to 60 nm.[2] Obviously, the resolution of lithographic technology has developed into nanometre-scale dimensions. The diffraction limit,[3] however, restricts the fabrication scale of conventional photolithography. Improvements of the resolution have been driven by decreasing the illumination wavelength. However, using short wavelength optics to reach the desired feature sizes will be confronted with more difficulties. For example, the extreme ultra-violet lithography (EUVL)[4] or the x-ray regime[5,6] requires new light sources, new optics, new resists and special mask, which will increase the cost of the IC fabrication and make the lithography complicated. Recently, photolithography in the optical near-field has been rapidly developed as a promising technique to fabricate high resolution features beyond the diffraction limit. Evanescent near-field lithography[7] has been successfully demonstrated for performing near-field photolithography. However, evanescent near-field lithography is limited by low transmission, short expose depth, and low contrast.[8] Surface plasmon polaritons (SPPs) are oscillations of surface electron charge density, which can be excited at the interface between prism and metal.[9,10] Using SPPs, the surface plasmon resonant interference nanolithography technique (SPRINT)[11] can successfully produce sub-wavelength pattern. However, this technique needs a grating with a very fine period as mask.

In this paper we present the feasibility analysis of a scheme based on maskless surface plasmon resonant lithography (MLSPRL) with prism coupling. The key idea in this scheme is to use a prism instead of metallic grating mask as a coupler, which makes the structure of lithographic system simple and reduces the cost of fabrication. Under the resonance condition, the intensity of electric field on the bottom side of the metallic film will be enhanced dramatically because of the coupling between SPPs and the evanescent. The effect of this enhancement can increase the depth of exposure, reduce exposure time and improve contrast as compared with the evanescent near-field lithography.

*Project supported by the National Basic Research of China (Grant No 2006CD302900-2), the National Natural Science Foundation of China (Grant No 60676024), and the Specialized Research Fund of China for the Doctoral Program of Higher Education (Grant No 20060610006).
†E-mail: dujinglei@tom.com

2. Basic configuration and principle of MLSPRL

A schematic of the MLSPRL process is shown in Fig.1. The uppermost layer is an isosceles triangle or hemispherical prism with a high refractive index, then a thin metal film is coated on the bottom surface of the prism, and finally they are brought into intimate contact with a thin resist covered on a substrate.[12]

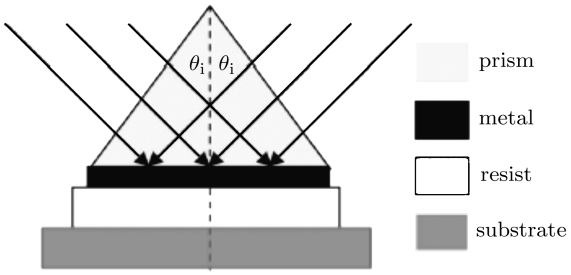


Fig.1. Schematic of the MLSPRL process.

When p-polarized light illuminates the interface between the prism and the metal film at the resonance angle, the momentum match between evanescence and SPPs will be satisfied. In this case, the reflectivity of illumination light reaches the lowest, and the intensity of the electromagnetic field below the metal film is enhanced dramatically. The coupling is recognized as attenuated total reflection (ATR) by which MLSPRL with high transmission and high contrast can be realized.

3. Theoretic analysis

3.1. Electric field distribution of single beam

In what follows, we analyse the electric field distribution below the metal film. Figure 2 describes the principle of surface plasmon resonance. For a p-polarized wave, there is no y dependence; we can describe the electromagnetic field below the metal film as follows:

$$E_3 = (E_{3x}, 0, E_{3z})\mathrm{e}^{\mathrm{i}(k_x x - k_{3z} z - \omega t)}, \quad (1)$$

$$H_3 = (0, H_{3y}, 0)\mathrm{e}^{\mathrm{i}(k_x x - k_{3z} z - \omega t)}, \quad (2)$$

where k_{3z} is the wave vector component parallel to the x direction below the metal film. It can be described by

$$k_{3z} = \left[\varepsilon_3 \left(\frac{\omega}{c}\right)^2 - k_x^2\right]^{\frac{1}{2}} = \frac{\omega}{c}\left(\frac{\varepsilon_3^2}{\varepsilon_2'(\omega) + \varepsilon_3}\right)^{\frac{1}{2}}, \quad (3)$$

where $\varepsilon_2'(\omega)$ is the real part of the metallic dielectric function, ε_3 is the dielectric constant of the resist, ω is the excitation frequency, k_x is the wave vector component of the electromagnetic field below the metal film along x direction, and[13]

$$k_x = \frac{\omega}{c}\sqrt{\varepsilon_2'(\omega)\varepsilon_3/[\varepsilon_2'(\omega) + \varepsilon_3]}. \quad (4)$$

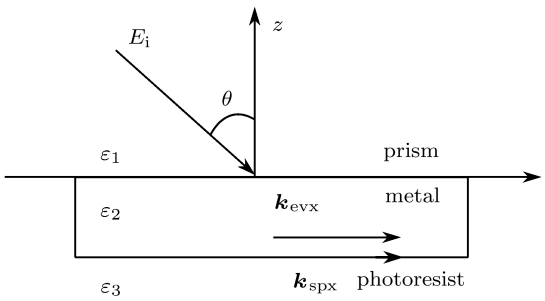


Fig.2. Schematic of surface plasmon resonance.

Obviously, the wave vector component k_{3z} is imaginary due to the relations $\varepsilon_3^2 > 0$ and $|\varepsilon_2'(\omega)| > \varepsilon_3$, so k_{3z} can be expressed as $k_{3z} = -\mathrm{i}\kappa$, where κ is a real number. Then

$$\begin{aligned} H_{3y} &= H_{3y}\mathrm{e}^{-\kappa z}\mathrm{e}^{\mathrm{i}(k_x x - \omega t)} \\ &= H_{3y}\mathrm{e}^{-\kappa z}\cos(k_x x - \omega t). \end{aligned} \quad (5)$$

Considering the relationship between electric field and magnetic field $\nabla \times \boldsymbol{H} = \varepsilon\dfrac{\partial \boldsymbol{E}}{\partial t}$ based on Maxwell's equations, the electric field can be described as

$$\begin{aligned} E_{3x} &= -\frac{k_{3z}H_{3y}}{\varepsilon_3\omega} \\ &= -\frac{\kappa}{\varepsilon_3\omega}H_{3y}\mathrm{e}^{-\kappa z}\sin(k_x x - \omega t), \end{aligned} \quad (6)$$

$$\begin{aligned} E_{3z} &= -\frac{k_x H_{3y}}{\varepsilon_3\omega} \\ &= -\frac{k_x}{\varepsilon_3\omega}H_{3y}\mathrm{e}^{-\kappa z}\cos(k_x x - \omega t). \end{aligned} \quad (7)$$

From Eqs.(6) and (7) we can find that the amplitudes of both E_{3x} and E_{3z} components decrease exponentially as $\exp(-\kappa z)$, and the amplitude ratio of E_{3z} to E_{3x} is given by

$$\frac{|E_{3z}|}{|E_{3x}|} = \frac{\left|\dfrac{-k_x}{\varepsilon_3\omega}H_{3y}\mathrm{e}^{-\kappa z}\right|}{\left|\dfrac{\kappa}{\varepsilon_3\omega}H_{3y}\mathrm{e}^{-\kappa z}\right|}$$

$$= \frac{|k_x|}{|\kappa|} = \frac{|k_x|}{|k_{3z}|} = \sqrt{\frac{|\varepsilon_2'(\omega)|}{\varepsilon_3}}. \quad (8)$$

Furthermore, we also find that there is a phase difference of $\frac{\pi}{2}$ between components E_{3x} and E_{3z}, which results in a half –period shift in space between the two components. The half-period shift will have a strong impact on the intensity contrast of the interference pattern. In order to reduce this effect, we should make the ratio $\frac{|E_{3z}|}{|E_{3x}|}$high enough.

3.2. Resolution of interference pattern

As shown in Fig.3, if two p-polarized waves illuminate the interface between prism and metal with equal intensity and symmetrical incident angle, the electric field intensities below the metal excited by these two illuminating light are equivalent. We assume that the electric intensity is expressed as

$$E_3 = (E_{3x}, 0, E_{3z})\mathrm{e}^{\mathrm{i}(k_x x - k_{3z} z - \omega t)}, \quad (9)$$

$$E_3' = (E_{3x}', 0, E_{3z}')\mathrm{e}^{\mathrm{i}(-k_x x - k_{3z} z - \omega t)}. \quad (10)$$

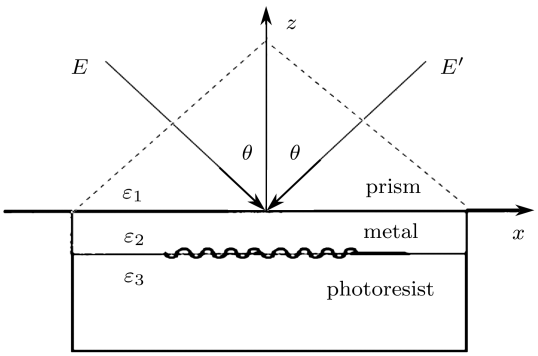


Fig.3. Schematic of interference of SPPs.

Then the electric field distribution in interference field can be given by

$$E_{\mathrm{inx}} = |E_{3x}|\mathrm{e}^{-\kappa z}\sin(2k_x x), \quad (11)$$

$$E_{\mathrm{inz}} = |E_{3z}|\mathrm{e}^{-\kappa z}\cos(2k_x x). \quad (12)$$

From Eqs.(11) and (12), we can see that the interference pattern of the two electric field components show sine distribution and cosine distribution, respectively. Moreover, we can write the period d of the interference pattern as follows:

$$d = \frac{2\pi}{2k_x} = \frac{\pi}{k_x}. \quad (13)$$

From Eqs.(4) and (13) we have

$$d = \pi\frac{c}{\omega}\sqrt{\frac{\varepsilon_2'(\omega) + \varepsilon_3}{\varepsilon_2'(\omega)\varepsilon_3}}. \quad (14)$$

Equation (14) demonstrates that the period d depends on the frequency of the illumination light, the dielectric constant of metal and photoresist. When metal and photoresist are specified, the pattern resolution only depends on the frequency of the illumination light under the resonance condition.

3.3. Enhancement factor

The enhancement effect is an important character in SPP interference lithography. Since the SPP is associated with evanescent wave, high intense electromagnetic fields confined to the metallic surface can be obtained. The value of the enhancement is given by the ratio of field intensity on the metal surface at the photoresist side divided by the incoming field intensity in the prism. The enhancement factor is related to the dielectric constant of metal, the thickness of metal film and the incident angle of illumination light. The enhancement of the electric field intensity can be obtained from[12]

$$T = \left|\frac{H_{\mathrm{en}}}{H_0}\right|^2 = \frac{t_{12}t_{23}\exp(\mathrm{i}k_{2z}d)}{1 + r_{12}r_{23}\exp(2\mathrm{i}k_{2z}d)}, \quad (15)$$

where r_{12} and r_{23} are the reflection coefficient of interface 1/2 and interface 2/3, respectively. The coefficient r_{ik} can be given by

$$r_{ik} = \frac{\dfrac{k_{iz}}{\varepsilon_i} - \dfrac{k_{kz}}{\varepsilon_k}}{\dfrac{k_{iz}}{\varepsilon_i} + \dfrac{k_{kz}}{\varepsilon_k}}. \quad (16)$$

Here t_{12} and t_{23} are the transmission coefficients of interface 1/2 and interface 2/3 respectively. The correlation between r_{ik} and t_{ik} can be described as

$$t_{ik} = 1 + r_{ik}. \quad (17)$$

From Eq.(15), the enhancement factor T is a function of the thickness d of the metallic film with the illumination wavelength being constant. For example, for illumination wavelengths of 441, 589 and 632 nm, the variations of the enhancement factor T with the thickness d of the metallic film are illustrated in Fig.4.

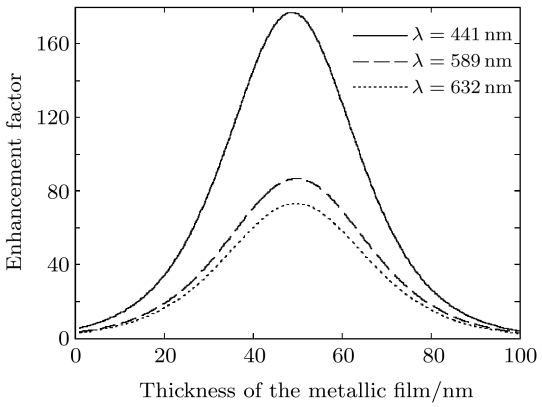


Fig.4. Enhancement factor as a function of the metallic film thickness.

As shown in Fig.4, though different enhancement factors can be obtained at different illumination wavelengths, it is advisable to select the prime thickness of 50nm to achieve the maximum enhancement factor for the three different wavelengths.

4. Results of numerical simulations

The behaviour of the electric field interference below the metal film can be simulated based on a finite-difference time-domain (FDTD) technique. Numerical values of refractive indices for the prism and the photoresist used in simulation are 1.94 and 1.53, respectively. The metal used is silver having the plasma frequency $\omega_{\rm p} = 9\,{\rm eV}$ and collision frequency $\gamma = 0.066\,{\rm eV}$; and the thickness of the silver film is 50 nm, and the incident angle of illumination light is 66.4°. Applying the perfectly matched layer method in our numerical model,[14] we obtained the simulation results as shown in Fig.5.

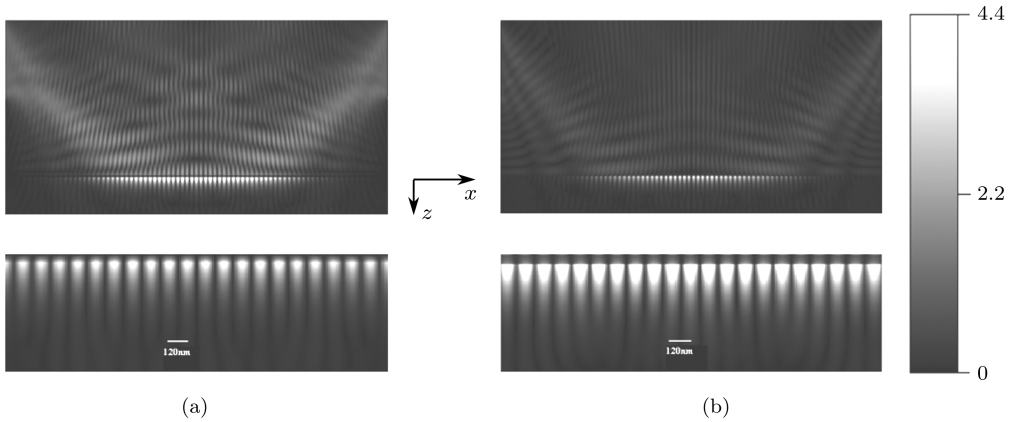


Fig.5. Electric field distribution of the interference patterns for E_z and E_x. (a) Electric field distribution of the interference patterns for E_z, (b) Electric field distribution of the interference patterns for E_x.

As can be seen from Fig.5, below the silver film SPP is excited and the electric field intensity is enhanced dramatically at the illumination wavelength $\lambda = 441\,{\rm nm}$. We notice that the fringes of E_z and E_x components have the same period which is approximately 120 nm and agrees well with the theoretical value 123.8 nm. If the line/space ratio is 1:1, the critical dimension of 60 nm can be produced, which is smaller than $\lambda/7$ and far departs from the diffraction limit of $\lambda/4$. In addition, we find that even though the fringes of E_z and E_x components have a half-period shift in space, the intensities of the E_z components are larger than those of the E_x components, which can provide sufficient intensity contrast. Figure 6 illustrates the intensity contrast defined by $V = (t^2 - 1)/(t^2 + 1)$ as a function of the distance from the origin. The contrast of the SPPs interference is approximately 0.6 within 200 nm depth, which can meet lithography purposes. In addition, we define the uniformity of exposure as

$$U = 1 - \frac{I_{\max} - I_{\min}}{I_{\max} + I_{\min}}, \tag{18}$$

where $I_{\max}$ and $I_{\min}$ are the maximum intensity and minimum intensity of bright fringes in the interference field. Then the uniformity exposure for both E_z and E_x components at different distances from the origin can be also described in Fig.6. Obviously, the uniformity of exposure for both E_z and E_x components are about 0.85 within 180 nm depth, which is sufficiently high for lithography.

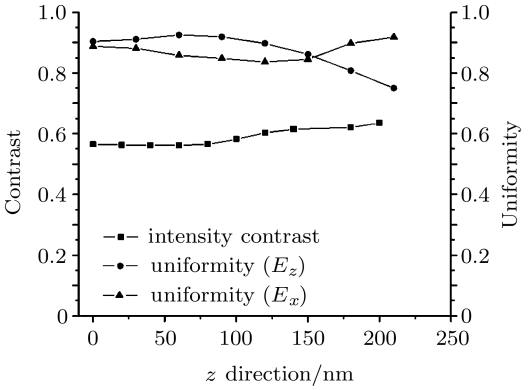


Fig.6. Intensity contrast and uniformity of exposure as functions of the distance from the origin.

Figure 7 demonstrates the normalized intensity $|H|^2/|H_0|^2$ distribution at different distances from origin along z direction, where $|H_0|^2$ is the intensity of the incident radiation. Obviously, the normalized intensity decays away from the origin, but the available expose depth can reach about 200 nm.

As is seen, near the origin the field intensity is about 20 times as strong as the incident intensity. It means that in this case the enhancement factor is 20 approximately, which is smaller than the theoretical analysis. We attribute this discrepancy to the designed incident angle calculated based on semi-infinite metal mould. Considering the difference between the semi-infinite metal and the finite thickness metal film, the designed incident angle is probably not the actual optimal angle. As a result, the enhancement factor fails to reach the maximum value.

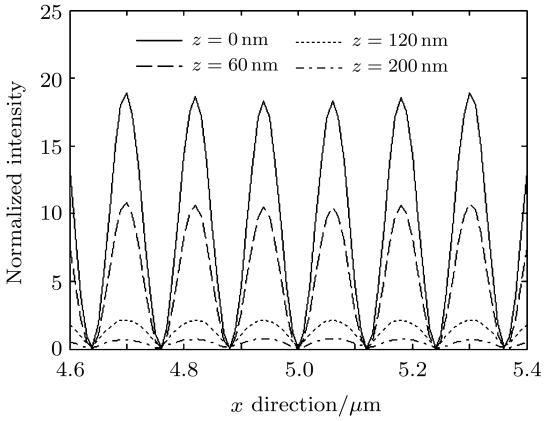


Fig.7. Normalized intensity distribution at different distances from origin along z direction.

5. Conclusions

In summary, we have demonstrated the maskless surface plasmon resonant interference lithography by discussing several important parameters, including period, enhancement factor, contrast and uniformity. The detailed theoretical analysis indicates the advantages of MLSPRL: such as high resolution, high contrast, low cost, and it provides a guideline for future experiments.

References

[1] Bondyopadhyay P K 1998 *Proc. IEEE* **86** 78
[2] Hamiltons 2003 *Computer* **36** 28
[3] Okazaki S 1991 *J. Vac. Sci. Technol.* B **9** 2829
[4] Gwyn C W, Stulen R, Sweeney D and Attwood D 1998 *J. Vac. Sci. Technol.* B **16** 3142
[5] Silverman J P 1998 *J. Vac. Sci. Technol.* B **16** 3137
[6] Yi F T, Ye T C, Peng L Q, Chen D P, Zhang J F and Han Y 2004 *Chin. Phys.* **13** 731
[7] Alkaisi M M, Blaikie R J, McNab S J, Cheung R and Cumming D R S 1999 *Appl. Phys. Lett.* **75** 3560
[8] Blaikie R J and McNab S J 2001 *Appl. Opt.* **40** 1692
[9] Bozhevolnyi S I and Pudonin F A 1997 *Phys. Rev. Lett.* **78** 2823
[10] Gao J X, Song G F, Guo B S, Gan Q Q and Chen L H 2007 *Acta Phys. Sin.* **56** 5827 (in Chinese)
[11] Luo X G and Ishihara T 2004 *Appl. Phys. Lett.* **84** 4780
[12] Guo X W, Du J L, Guo Y K and Yao J 2006 *Opt. Lett.* **31** 2613
[13] Raether H 1988 *Surface Plasmons on Smooth and Rough Surfaces and on Gratings* (New York: Springer) p5
[14] Berenger J P 1994 *Comput. Phys.* **114** 185